

Experimental study of secure quantum key distribution with source and detection imperfections

Ye Chen,¹ Chunfeng Huang,¹ Zihao Chen,¹ Wenjie He,¹ Chengxian Zhang,¹ Shihai Sun^{2†} and Kejin Wei^{1,*}

¹*Guangxi Key Laboratory for Relativistic Astrophysics,
School of Physical Science and Technology,
Guangxi University, Nanning 530004, China*

²*School of Electronics and Communication Engineering,
Sun Yat-Sen University, Shenzhen 518107, China*

[†]*sunshh8@mail.sysu.edu.cn*

^{*}*kjwei@gxu.edu.cn*

(Dated: August 9, 2022)

The quantum key distribution (QKD), guaranteed by the principle of quantum physics, is a promising solution for future secure information and communication technology. However, device imperfections compromise the security of real-life QKD systems, restricting the wide deployment of QKD. This study reports a decoy-state BB84 QKD experiment that considers both source and detection imperfections. In particular, we achieved a rigorous finite-key security bound over fiber links of up to 75 km by applying a systematic performance analysis. Furthermore, our study considers more device imperfections than most previous experiments, and the proposed theory can be extended to other discrete-variable QKD systems. These features constitute a crucial step toward securing QKD with imperfect practical devices.

I. INTRODUCTION

Quantum key distribution (QKD) has attracted significant interest as an information-theoretic security communication technology. With numerous effort, QKD has been widely proven in theory [1–3] and has been experimentally demonstrated in different scenarios, such as fiber-based [4–9] and free-space channels [10–12]. Various QKD networks have been reported worldwide [13–18]. Recently, the QKD distance has been increased to 830 km for fiber spools [19] based on twin-field QKD [20].

The security of QKD is guaranteed, assuming that the features of real-life devices are in line with the theoretical models in security proofs [21]. However, the existing imperfections in practical components bridge a gap between theory and practice. This aspect has opened several considerable loopholes to eavesdropping by the eavesdropper (Eve). Indeed, several quantum hacking attacks exploiting such realistic security loopholes have been reported [22–27]. See [28–31] for a literature review involving this topic.

To recover the security of actual QKD implementations, several important approaches, such as device-independent QKD [32–34], measurement-device-independent QKD [35, 36], and security patch, were proposed. Among them, the “security patch” method, which monitors the parameters for imperfections of the system and considers these in a detailed (GLLP-style) security analysis, has attracted increasing interest. This method usually requires to modify the hardware or post-processing process in the current system. Following this line, several studies have been conducted focusing on different imperfections in the security proof, such as detection mismatch [37, 38], source flaws [39–42], Trojan-horse [43], pattern effects [24], polarization-dependent loss [44], and distinguishable decoy states [45]. Experi-

mental demonstrations of QKD using such refined security proofs have also been reported [46–50]. However, in most previous studies, the flaws were considered individually using different models.

To overcome this problem, Sun and Xu [51] recently proposed a systematic performance analysis that considers both source and detection imperfections in one model. With this systematic performance analysis, legitimate users can achieve considerable secure key bits over long distances by measuring the required parameters to quantify the flaws of devices in real-life QKD systems. Nevertheless, a QKD experiment that implements such an advanced theory has yet to be completed. Furthermore, in [51], the authors only applied it to a two-decoy-state case assuming that an arbitrarily large number of signals could be used for evaluating the final key bits. However, this assumption is unrealistic because QKD systems typically run in a limited time without an arbitrarily large number of received pulses. In addition, the distilled key is highly affected by statistical fluctuations. Therefore, the practicality of this protocol remains unknown.

In this study, we present an experimental demonstration of decoy-state BB84 QKD by considering most source and detection imperfections. Our demonstration exploits the refined security proof in [51], which only requires one decoy state and considers the finite-data-size effect. Furthermore, with the refined security proof, we successfully distribute secure key bits over different fibers by considering additional device imperfections. The theoretical and experimental contributions of this study are detailed below.

Theoretically, we present a refined version of that presented in [51]. The refined version requires only one decoy-state and finite signals for the parameter estimation. Note that because implementing one decoy is eas-

ier, and the one-decoy-state method outperforms the two-decoy-state method in most of experimental settings [52], our analysis is crucial for integrating the security proof into a practical QKD system and completing the demonstration of the advanced theory.

Experimentally, contrasting to previous BB84 QKD demonstrations that do not individually consider source and detection imperfections, we carefully quantify the detection efficiency mismatch and almost all source imperfections, including inaccurate state preparation, distinguishable decoy states, and Trojan horses. Moreover, we consider the secret key rate estimation together. Finally, we successfully distributed secure key bits over up to 75 km of a commercial fiber spool.

The remainder of this paper is organized as follows. In Sec. II, we review the security proof in [51] and then present the one-decoy-state scheme in Sec. III. In Sec. IV, we illustrate our experimental setup and show the results. Finally, we summarize the study in Sec. V.

II. PROTOCOL

In [51], the authors used a systematic security model that considered almost all source flaws and detector efficiency mismatches. Based on the main results in [51], considering that a weak coherent source is used, the final key rate can be written as follows:

$$R \geq P_{succ} \mu e^{-\mu} Y_1^\mu [1 - H(\delta_{p,1}^{z,\mu})] - Q_\mu f_{EC} H(E_\mu), \quad (1)$$

where P_{succ} is the probability of Bob's successful execution of the virtual X -measurement, a coefficient less than 1; μ is the intensity of the signal state; Y_1^μ and $\delta_{p,1}^{z,\mu}$ are the single-photon yield and single-photon phase error rate, respectively; f_{EC} is the error correction efficiency. Q_μ and E_μ are the total gain and the bit error rate of the signal state, respectively; and $H(x)$ represents the binary information entropy function.

To accurately estimate the lower bound of the key rate, the legitimate users should bound Eve's information by numerically searching the following routine:

$$\begin{aligned} \underset{\rho_E}{Max} : \delta_{p,1}^{z,\mu} \quad \text{and} \quad \underset{\rho_E}{Min} : P_{succ} \\ \text{Subject to : } \delta_{b,1}^{x,\mu}, \delta_{b,1}^{z,\mu}, P_{ij,1}^{\beta\beta'} \end{aligned} \quad (2)$$

where $\delta_{b,1}^{z(x),\mu}$ denotes the single-photon bit error rate in $Z(X)$ -basis; $P_{ij,1}^{\beta\beta'}$, $\{i, j\} \in \{0, 1\}$, and $\{\beta, \beta'\} \in \{z, x\}$ represent the probability that Alice sends a single-photon quantum state associated with bit " i " in β -basis and Bob obtains bit " j " in β' -basis. All of the above factors can be estimated by decoy-state analysis [53, 54].

The values of device imperfections are connected to key rate formulas by incorporating them into the con-

strictions, which satisfy the following equation:

$$\begin{aligned} P_{ij,1}^{zz} &= \text{Tr} \left\{ \rho_E \left[(f_{z_i} \otimes Z_{ij})^+ f (f_{z_i} \otimes Z_{ij}) \right] \otimes F_j^+ F_j \right\} \\ P_{ij,1}^{xx} &= \text{Tr} \left\{ \rho_E \left[(f_{x_i} \otimes X_{ij})^+ f (f_{x_i} \otimes X_{ij}) \right] \otimes F_j^+ F_j \right\} \\ P_{ij,1}^{xx, vir} &= \frac{1}{4} \text{Tr} \left\{ \rho_E (Z_{ij}^p \otimes C^+ C) \right\}, \end{aligned} \quad (3)$$

where $\rho_E = |\xi(i)\rangle\langle\xi(i)|$ denotes the density matrix of Eve's POVM operators, f_{z_i} (f_{x_i}) is a diagonal matrix that denotes the fidelity of the side channel state, Z_{ij} (X_{ij}) is the coding accuracy of the encoded quantum state in the $Z(X)$ -basis, and $F_j^+ F_j$ is the detection efficiency matrix of the detector. C is a dummy filter for estimating the phase error rate, which can be constructed using $F_j^+ F_j$. Based on [51], Eq. (3) can be further derived as follows:

$$\begin{aligned} \delta_{b,1}^{z,\mu} &= \frac{P_{10,1}^{zz} + P_{01,1}^{zz}}{P_{00,1}^{zz} + P_{01,1}^{zz} + P_{10,1}^{zz} + P_{11,1}^{zz}} \\ \delta_{b,1}^{x,\mu} &= \frac{P_{10,1}^{xx} + P_{01,1}^{xx}}{P_{00,1}^{xx} + P_{01,1}^{xx} + P_{10,1}^{xx} + P_{11,1}^{xx}} \end{aligned} \quad (4)$$

$$\delta_{p,1}^{z,\mu} = \frac{P_{10,1}^{xx, vir} + P_{01,1}^{xx, vir}}{P_{00,1}^{xx, vir} + P_{01,1}^{xx, vir} + P_{10,1}^{xx, vir} + P_{11,1}^{xx, vir}}$$

$$P_{succ} = \frac{P_{00,1}^{xx, vir} + P_{01,1}^{xx, vir} + P_{10,1}^{xx, vir} + P_{11,1}^{xx, vir}}{P_{00,1}^{zz} + P_{01,1}^{zz} + P_{10,1}^{zz} + P_{11,1}^{zz}}.$$

Here the superscript *vir* in $P_{ij,1}^{xx, vir}$ represents the virtual X -basis. Hence, legitimate users can first measure the required parameters in a real-life QKD system and numerically find the required parameters for evaluating the final key rate by performing the routine of Eq. (2), under the constraints given in Eqs. (3) and (4). Finally, the final key rate can be evaluated by inputting the obtained parameters into Eq. (1). The model of imperfections from the measured parameters can be found in Appendix A. We remark that the framework of this security proof has a similar routine of recent well-established numerical approach [55, 56].

III. ONE-DECOY METHOD AND FINITE-SIZE ANALYSIS

In [51], the parameters in Eq. (1) were estimated using the two-decoy-state method without considering the finite size effect. Hence, this approach has a relatively complex implementation and requires infinite data for parameter estimation, challenging to perform experimentally. Here, we present a refined version requiring only one decoy state [52] and finite signals for parameter estimations. The proposed method significantly reduces

the experimental complexity. Based on the method presented in [52], the final secure key is expressed as

$$l \geq s_{z,0}^L + P_{succ} s_{z,1}^L (1 - h(\delta_{p,1}^{z,\mu})) - \lambda_{EC} - 6 \log_2 \frac{19}{\varepsilon_{sec}} - \log_2 \frac{2}{\varepsilon_{cor}}, \quad (5)$$

where $s_{z,0}^L$ is the lower bound of the detection counts when Alice sends a vacuum state in the Z -basis and is detected by Bob, $s_{z,1}^L$ is the lower bound of the single-photon detection counts in the Z -basis, λ_{EC} is the number of bits consumed in error correction, and $\varepsilon_{sec} = 10^{-9}$ and $\varepsilon_{cor} = 10^{-15}$ are the secrecy and correctness factors, respectively.

When considering the finite-data effect and the distinguishable decoy states based on the analysis presented in [51, 52], $s_{z,0}^L$ and $s_{z,1}^L$ can be estimated using the following expression:

$$\begin{aligned} s_{z,0}^L &= \max \left\{ \frac{1}{\mu - \nu} [\mu n_{z,\nu}^- - \nu n_{z,\mu}^+ - 2N_{zz} D_{\mu\nu} \mu (e^\nu - 1)], \right. \\ &\quad \left. \frac{1}{\mu - \nu} [\mu n_{z,\nu}^- - \nu n_{z,\mu}^+ - 2N_{zz} D_{\mu\nu} \nu (e^\mu - 1)], 0 \right\} \\ s_{z,1}^L &= \frac{\tau_1 \mu}{\nu(\mu - \nu)} \left(n_{z,\nu}^- - \frac{\nu^2}{\mu^2} n_{z,\mu}^+ - \right. \\ &\quad \left. \frac{(\mu^2 - \nu^2)}{\mu^2} \frac{s_{z,0}^U}{\tau_0} - 2N_{zz} D_{\mu\nu} (e^\nu - e^{\nu(1-\eta_{Bob}^{cal})}) \right), \end{aligned} \quad (6)$$

where $\eta_{Bob}^{cal} = \eta_{Bob} \times \eta_d$. In addition, η_{Bob} is the total transmittance of Bob, and η_d is detection efficiency. N_{zz} is the total number of pulses that Alice sends to the quantum state in the Z -basis and Bob successfully detects in the Z -basis. τ_i is the probability of sending i photons, and μ and ν represent the intensity of signal state and decoy state respectively. Finally, $n_{z,k}^\pm$ is the finite-key correction of the counts in the Z -basis with respect to the intensity $k \in \{\mu, \nu\}$, estimated using Hoeffding's inequality as follows:

$$n_{z,k}^\pm = \frac{e^k}{p_k} \left(n_{z,k} \pm \sqrt{\frac{n_z}{2} \log \frac{1}{\varepsilon_1}} \right), \quad (7)$$

where p_k is the probability choice for intensity k , n_z is the total count in the Z -basis, and $s_{z,0}^U$ is the upper bound on vacuum events, which can be evaluated by

$$s_{z,0}^U = 2 \left(\frac{e^k}{p_k} m_{z,k}^+ + \sqrt{\frac{n_z}{2} \log \frac{1}{\varepsilon_1}} \right), \quad (8)$$

where the estimate of $m_{z,k}^+$ is similar to Eq. (7), which can be determined as follows:

$$m_{z,k}^\pm = \frac{e^k}{p_k} \left(m_{z,k} \pm \sqrt{\frac{m_z}{2} \log \frac{1}{\varepsilon_2}} \right). \quad (9)$$

Here, ε_i denotes the failure probability of the finite-size analysis, $i \in \{1, 2\}$. To numerically search P_{succ} and $\delta_{p,1}^{z,\mu}$, we need to perform decoy analysis to obtain the constraints of Eq. (4). When considering the finite data effect, Eq. (4) can be rewritten as follows:

$$\delta_{b,1}^{z,\mu} \leq \frac{T_{z,0,1}^U + T_{z,1,1}^U}{s_{z,1,1}^L + s_{z,0,1}^L}, \quad \delta_{b,1}^{x,\mu} \leq \frac{T_{x,0,1}^U + T_{x,1,1}^U}{s_{x,1,1}^L + s_{x,0,1}^L}, \quad (10)$$

Here, we used the following relation:

$$\begin{aligned} T_{z(x)0,1} &= N_{zz(xx)} P_{01,1}^{zz(xx)} \\ T_{z(x)1,1} &= N_{zz(xx)} P_{10,1}^{zz(xx)} \\ s_{z(x)0,1} &= N_{zz(xx)} \left[P_{00,1}^{zz(xx)} + P_{01,1}^{zz(xx)} \right] \\ s_{z(x)1,1} &= N_{zz(xx)} \left[P_{10,1}^{zz(xx)} + P_{11,1}^{zz(xx)} \right], \end{aligned} \quad (11)$$

where $s_{\beta_i,1}$ denote the counts that Alice sends a single-photon quantum state associated with bit “ i ” in β -basis; $s_{\beta_i,1}$ can be estimated using one-decoy state method using following equations [50]:

$$\begin{aligned} s_{\beta_i,1} \geq s_{\beta_i,1}^L &= \frac{\tau_1 \mu}{\nu(\mu - \nu)} \left(n_{\beta_i,\nu}^- - \frac{\nu^2}{\mu^2} n_{\beta_i,\mu}^+ - \right. \\ &\quad \left. \frac{(\mu^2 - \nu^2)}{\mu^2} \frac{s_{\beta_i,0}^U}{\tau_0} - 2N_{\beta_i\beta'} D_{\mu\nu} (e^\nu - e^{\nu(1-\eta_{Bob}^{cal})}) \right), \end{aligned} \quad (12)$$

where $n_{\beta_i,k}^\pm$ denotes the upper and lower bound of the counts $n_{\beta_i,k}$, $N_{\beta_i\beta'}$ represents the counts when the total number of pulses that Alice sends the quantum state in β -basis with bit “ i ” and Bob detects in the β' -basis. Moreover, $n_{\beta_i,k}$ can be directly obtained experimentally, $T_{\beta_i,1}^U$ is the upper bound of single-photon error counts $T_{\beta_i,1}$ given that Alice sends a single-photon quantum state associated with bit “ i ” in β -basis, which can be estimated as follows:

$$T_{\beta_i,1} \leq T_{\beta_i,1}^U = \min\{K_m^\mu, K_m^\nu, K_m^{\mu\nu}\},$$

$$K_m^\mu = \frac{\tau_1 (m_{\beta_i,\mu}^+ - e_0 s_{\beta_i,0}^L)}{\mu},$$

$$K_m^\nu = \frac{\tau_1 (m_{\beta_i,\nu}^+ - e_0 s_{\beta_i,0}^L + 2N_{\beta_i\beta'} \nu D_{\mu\nu} \eta_{Bob}^{cal})}{\nu},$$

$$K_m^{\mu\nu} = \frac{\tau_1 \left[m_{\beta_i,\mu}^+ - m_{\beta_i,\nu}^- + 2N_{\beta_i\beta'} D_{\mu\nu} (e^\nu - e^{\nu(1-\eta_{Bob}^{cal})}) \right]}{\mu - \nu}. \quad (13)$$

IV. EXPERIMENT

We implemented the above protocol using a custom-made polarization-encoding BB84 QKD system [57]. The

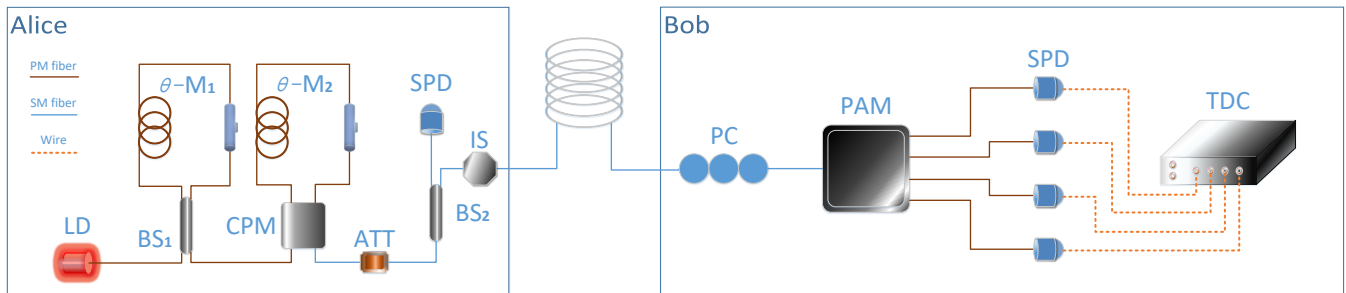


FIG. 1. Schematic diagram of the BB84 QKD experimental setup. LD: commercial laser diode; BS₁: beam splitter of 75:25; BS₂ beam splitter of 50:50; θ -M_i: phase modulator; CPM: customized polarization module; ATT: optical attenuator; IS: optical isolation; PC: polarization controller; SPD: single-photon avalanche detector; PAM: polarization analysis module; TDC: time-to-digital converter. Polarization-maintaining fiber is used at both receiving and sending terminals.

TABLE I. Required parameters for the considered imperfections, δ_{β_i} is the modulation error in the source, $D_{\mu\nu}$ is the distance between the signal and decoy states, μ_{out} is the intensity of reflected Trojan-horse photon, and $F_j^+ F_j$, $j \in \{0, 1\}$ is the detection efficiency matrices of detector for bit “ j ”. In an ideal QKD system, the values of the required parameters are equal to zero in the first three imperfections, and the detection efficiency matrices are an identity matrix.

Considered imperfection		Flaws parameters
Inaccuracy of the encoded state	$\delta_{z_0} = 0$, $\delta_{z_1} = 0.0726$, $\delta_{x_0} = 0.0891$, $\delta_{x_1} = 0.0285$	
Distinguishable decoy states		$D_{\mu\nu} = 1.6 \times 10^{-3}$
Trojan-horse		$\mu_{out} = 3.6 \times 10^{-10}$
Detection mismatch	$F_0^+ F_0 = \text{diag}[1, 0.6621]$, $F_1^+ F_1 = \text{diag}[0.3354, 1]$	

system was realized using commercially available components with an up-gradation of security and stability. We note that our method is general and can be applied to other BB84 QKD systems. Here, we implement the developed homemade system through a case study.

A. Setup

A schematic of the experimental setup is shown in Fig. 1. Alice used commercial lasers (LD, WT-LD200-DL, Qasky Co. LTD) to generate light pulses with a frequency of 50 MHz. The emitted light pulses were first fed into a Sagnac-based intensity modulation (Sagnac IM) to actively generate two intensities for the one-decoy method. Subsequently, the light pulse passed through Sagnac-based polarization modulation (Sagnac PM). A pre-calibration voltage was applied to a phase modulator using an arbitrary waveform generator (AWG) to produce standard BB84 polarization states. After that, the modulated light pulses were attenuated to the single-photon level using an attenuator (ATT). A cascaded optical isolator (IS), with an isolation of 180.3 dB, was used in the output of Alice’s station to prevent a Trojan-horse attack.

At the receiving station Bob, a polarization controller (PC) was used to actively compensate for the polarization drift during transmission over the fiber channels. The received quantum states were decoded using a polarization decoding module (PAM) and detected by four infrared InGaAs single-photon detectors

(SPDs, WT-SPD2000, Qasky Co. LTD). The average efficiency of SPDs was approximately 8.5%, and the dark count rate was 10^{-6} . Electrical signals from the detector were recorded using a time digital converter (TDC, quTDC100, GmbH), which was then processed by a computer. After careful calibration of the system, an optical misalignment error rate of 1% was obtained.

B. Implementation

We first experimentally quantified the required parameters for the considered imperfections in the proposed security proof, including the inaccuracy of the encoded quantum state, distinguishable decoy states, Trojan-horse, and detection efficiency mismatch. The measurement results are summarized in Table I, and the detailed measurement for each imperfection and the incorporation of such parameters into the security proof can be found in Appendix A.

We successfully implemented our protocol in the finite-key regime over a commercial fiber at 25 km, 50 km, and 75 km. We optimized the implementation parameters by considering the measurement results of the evaluated imperfections. Moreover, we obtained the optimal implementation parameters, including the intensities of the signal and decoy states and the probabilities of sending them for each distance. For example, our optimized parameters for 75 km were $\mu = 0.40$, $\nu = 0.10$, and $P_\mu = 0.84$. Further details of the implemented parameters for each distance are listed in Table II.

TABLE II. Implemented parameters and experimental results. $Loss$ is the channel loss, N denotes the total number of pulses, μ and ν are the intensity of the signal state and the decoy state, respectively. P_μ is the probability of the signal state, P_ν is the probability of the decoy state, E_μ is the bit error rate of the signal state, and l is the secret key rate.

Channel		Parameters					Results			
$L(km)$	$Loss(dB)$	N	μ	ν	P_μ	P_ν	P_{succ}	$\delta_{p,1}^{z,\mu}$	E_μ	l
25	4.736	1.00653×10^{10}	0.45	0.1125	0.84	0.16	0.5360	0.0243	1.11%	8.738×10^4
50	9.602	1.00365×10^{10}	0.43	0.1075	0.76	0.24	0.5946	0.0525	1.03%	1.955×10^4
75	15.08	1.00481×10^{10}	0.40	0.1000	0.54	0.46	0.5601	0.1745	1.34%	7.729×10^2

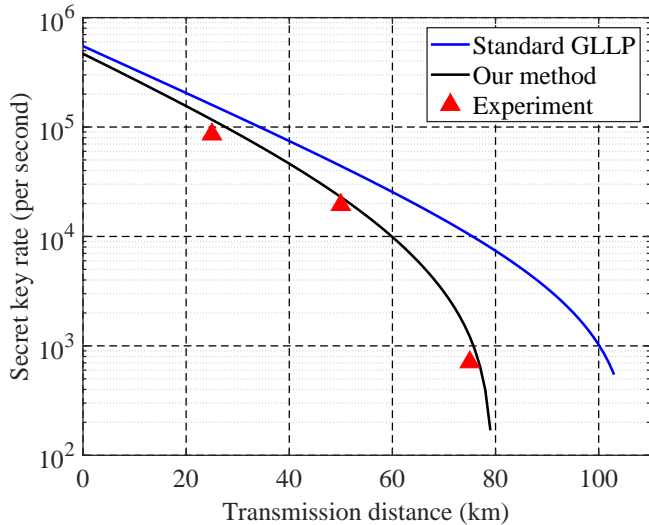


FIG. 2. Experimental secret key rates (red triangle) over fiber lengths of 25, 50, and 75 km. The black (lower) and blue (upper) lines represent the simulated secret key rate using the proposed method and the standard GLLP analysis without considering imperfections.

For each distance, a total of $N = 10^{10}$ was sent. We collected all counts and post-processed the data for the secret key rate estimations. Detailed raw data are provided in Appendix B. The obtained quantum bit error rate of our system was below 1.5%. Substituting the experimental data into the one-decoy method presented in Sec. III and performing the numerical search routine of Eq. (2), we got the experimental results listed in Tab. II. The results are shown in Fig. 2. Based on the proposed security proof, we can distill a secret key rate of 773 bps at a distance of up to 75 km. The security of these keys considered almost all source flaws and detection mismatch.

In addition, we obtained the simulation results using standard GLLP analysis without considering any imperfections for comparison purposes. The simulation exploited the experimental parameters of the proposed setup, and the parameters for the decoy-state method were optimized. As shown in Fig. 2, because the proposed approach considers more imperfections, our method has an acceptable penalty for the obtained secret key rate and the achievable distance.

V. CONCLUSION

We developed a decoy-state BB84 QKD experiment that considered almost all source flaws and detection mismatches. The study relied on the security proof reported in [51] with a simpler decoy method and considering the finite-size effect. Finally, we successfully generated secure key bits of 773 bps in fiber links up to 75 km. Compared with previous experiments that only considered a single flaw, our results proved the feasibility of distributing secure key bits over a long distance, jointly considering source and detection imperfections.

Our method, including parameter estimations, finite-key analysis, the quantification of device imperfections, and the implement, is general. Hence, it is a interesting future research that applies the proposed method to other QKD systems, such as a chip-based system [59, 60], to improve the security of key bits. Furthermore, considering the obtained key rate has a certain reduction compared with GLLP analysis without considering imperfections. It would be interesting to improve the secret key rate by introducing state-of-art techniques. For example, in our work, we exploited one-decoy method because of easy implementation. introducing two-decoy method, which has been proved to provide a tighter bound than one-decoy method, would an efficient way; Ref. [40, 63] provides a loss tolerant protocol which has a better performance than the traditional GLLP analysis with leaky source. It is possible to use the loss tolerant protocol to make the key rate performance better.

VI. ACKNOWLEDGMENTS

This study was supported by the National Natural Science Foundation of China (Nos. 62171144, 62031024, and 62171485), the Guangxi Science Foundation (No. 2021GXNSFAA220011), and the Open Fund of IPOC (BUPT) (No. IPOC2021A02).

Appendix A: The details of quantifying the considered imperfections

In this appendix, we present the proposed method for measuring the required parameters to quantify the considered imperfections. In addition, we describe how to

TABLE III. Raw data and modulation errors for state preparation. The detection efficiencies of detector 1 (2) are 8.25% and 8.76%, respectively.

Polarization	θ	$D_{1,\theta}$	$D_{2,\theta}$	$\delta_{\beta_i}^U$
$H(z_0)$	0	824	348092	/
$P(x_0)$	$\pi/2$	146280	207533	0.0726
$V(z_1)$	π	285143	3244	0.0891
$M(x_1)$	$3\pi/2$	159280	189432	0.0285

construct the density matrix used in the security proof.

1. Inaccuracy of encoded state

We quantified the inaccuracy of the encoded state by measuring the modulation error δ_{β_i} in the Sagnac PM, as shown in Fig. 1. θ_{β_i} is defined as the difference between the applied and ideal phases $\theta \in \{0, \pi/2, \pi, 3\pi/2\}$ when preparing the state $\beta_i, \beta \in \{z, x\}, i \in \{0, 1\}$. In particular, the process is as follows. First, we determine the optimal voltages for modulating the expected polarizations following a custom calibration procedure. Subsequently, Alice connects directly to Bob via an attenuator. Subsequently, Alice scans the optimal voltages to her Sagnac-based polarization modulator and records the detection counts of the two detectors in the Z -basis measurement. These counts are represented by $D_{1,\theta}$ and $D_{2,\theta}$. The measurement results are listed in Tab. III.

The upper bound of δ_{β_i} is given as follows:

$$\delta_{\beta_i} \leq \delta_{\beta_i}^U = \frac{1}{2} \left| \theta - 2 \arctan \left(\sqrt{\frac{(D_{1,\theta}^+ - D_{1,0}^-) / \eta_{d1}}{(D_{2,\theta}^- - D_{1,0}^+) / \eta_{d2}}} \right) \right| \quad (\text{A1})$$

where $D_{i,\theta}^\pm = D_{i,\theta} \pm \sqrt{D_{i,\theta} / 2 \ln(1/\varepsilon)}$ denotes the lower and upper bounds of $D_{i,\theta}$, which is bounded by Hoeffding's inequality, and $\eta_{d1} = 8.25\%$ and $\eta_{d2} = 8.76\%$ are the detection efficiencies of the two detectors. We set $\varepsilon = 10^{-10}$.

To construct the density matrix Z_{ij} and X_{ij} used in Eq. (3) according to [51], the state-preparation flaw parameter is defined as follows:

$$\varepsilon_{\beta_i} = \sin^2(\delta_{\beta_i}) / \eta_c, \quad (\text{A2})$$

where η_c denotes channel loss. Subsequently, by inputting δ_{β_i} into Eq. (A2), we obtain the coding accuracy

matrices Z_{ij} , expressed as follows:

$$\begin{aligned} Z_{00} &= \begin{bmatrix} \sqrt{1 - \varepsilon_{z_0}} & \sqrt{\varepsilon_{z_0}} & 0 & 0 \\ 1 & 0 & 0 & 0 \end{bmatrix} \\ &= \begin{bmatrix} 1 & 0 & 0 & 0 \end{bmatrix} \end{aligned}$$

$$\begin{aligned} Z_{01} &= \begin{bmatrix} 0 & 0 & \sqrt{1 - \varepsilon_{z_0}} & \sqrt{\varepsilon_{z_0}} \\ 0 & 0 & 1 & 0 \end{bmatrix} \\ &= \begin{bmatrix} 0 & 0 & 1 & 0 \end{bmatrix} \end{aligned}$$

$$\begin{aligned} Z_{10} &= \begin{bmatrix} \sqrt{\varepsilon_{z_1}} & \sqrt{1 - \varepsilon_{z_1}} & 0 & 0 \\ \sqrt{7.9 \times 10^{-3} / \eta_c} & \sqrt{1 - 7.9 \times 10^{-3} / \eta_c} & 0 & 0 \end{bmatrix} \\ &= \begin{bmatrix} \sqrt{7.9 \times 10^{-3} / \eta_c} & \sqrt{1 - 7.9 \times 10^{-3} / \eta_c} & 0 & 0 \end{bmatrix} \end{aligned}$$

$$\begin{aligned} Z_{11} &= \begin{bmatrix} 0 & 0 & \sqrt{\varepsilon_{z_1}} & \sqrt{1 - \varepsilon_{z_1}} \\ 0 & 0 & \sqrt{7.9 \times 10^{-3} / \eta_c} & \sqrt{1 - 7.9 \times 10^{-3} / \eta_c} \end{bmatrix}. \end{aligned} \quad (\text{A3})$$

The density matrix of the X -basis can be obtained using the transpose matrix U similarly to Z_{ij} , which is expressed as follows:

$$\begin{aligned} X_{00} &= \begin{bmatrix} \sqrt{1 - \varepsilon_{x_0}} & \sqrt{\varepsilon_{x_0}} & 0 & 0 \\ \sqrt{1 - 5.3 \times 10^{-3} / \eta_c} & \sqrt{5.3 \times 10^{-3} / \eta_c} & 0 & 0 \end{bmatrix} \times U \\ &= \begin{bmatrix} \sqrt{1 - 5.3 \times 10^{-3} / \eta_c} & \sqrt{5.3 \times 10^{-3} / \eta_c} & 0 & 0 \end{bmatrix} \times U \end{aligned}$$

$$\begin{aligned} X_{01} &= \begin{bmatrix} 0 & 0 & \sqrt{1 - \varepsilon_{x_0}} & \sqrt{\varepsilon_{x_0}} \\ 0 & 0 & \sqrt{1 - 5.3 \times 10^{-3} / \eta_c} & \sqrt{5.3 \times 10^{-3} / \eta_c} \end{bmatrix} \times U \\ &= \begin{bmatrix} 0 & 0 & \sqrt{1 - 5.3 \times 10^{-3} / \eta_c} & \sqrt{5.3 \times 10^{-3} / \eta_c} \end{bmatrix} \times U \end{aligned}$$

$$\begin{aligned} X_{10} &= \begin{bmatrix} \sqrt{\varepsilon_{x_1}} & \sqrt{1 - \varepsilon_{x_1}} & 0 & 0 \\ \sqrt{8.1 \times 10^{-4} / \eta_c} & \sqrt{1 - 8.1 \times 10^{-4} / \eta_c} & 0 & 0 \end{bmatrix} \times U \\ &= \begin{bmatrix} \sqrt{8.1 \times 10^{-4} / \eta_c} & \sqrt{1 - 8.1 \times 10^{-4} / \eta_c} & 0 & 0 \end{bmatrix} \times U \end{aligned}$$

$$\begin{aligned} X_{11} &= \begin{bmatrix} 0 & 0 & \sqrt{\varepsilon_{x_1}} & \sqrt{1 - \varepsilon_{x_1}} \\ 0 & 0 & \sqrt{8.1 \times 10^{-4} / \eta_c} & \sqrt{1 - 8.1 \times 10^{-4} / \eta_c} \end{bmatrix} \times U, \end{aligned} \quad (\text{A4})$$

and

$$U = \frac{1}{2} \begin{bmatrix} 1 & 1 & 1 & 1 \\ 1 & -1 & 1 & -1 \\ 1 & 1 & -1 & -1 \\ 1 & -1 & -1 & 1 \end{bmatrix}. \quad (\text{A5})$$

Note that similar methods have been used to quantify the modulation errors in a BB84 phase-encoding system [46], a polarization-encoding measurement-device-independent system [47], and the polarization-dependent loss in a BB84 polarization-encoding system [50].

2. Distinguishable decoy state

In our setup, the signal and decoy states are modulated by Sagnac IM, as shown in Fig. 1. The splitter ratio of BS₁ was set to 75 : 25. By applying the phase 0 or π to the θ -M₁, a signal state and decoy state with an intensity ratio of 4:1 were generated. To quantify the parameters of the distinguishable decoy states of the intensity

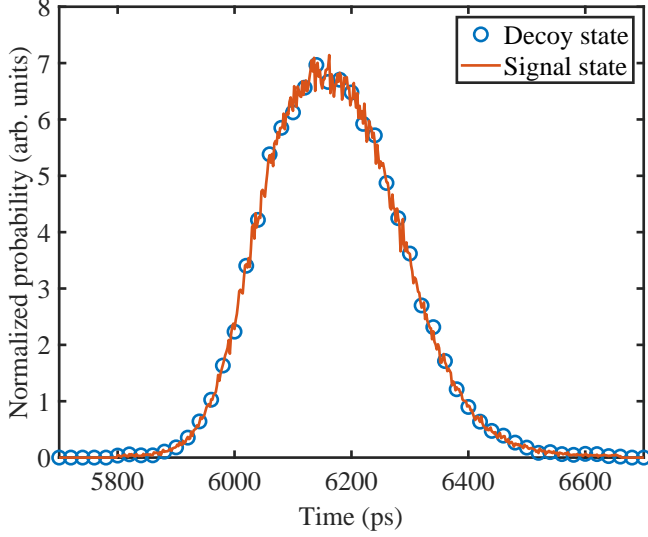


FIG. 3. Normalized intensity distribution of the signal state and the decoy state in the time domain. The red line and blue circle represent the signal state and decoy state, respectively. For comparison purposes, the signal state and decoy state were normalized to have the same area. The signal-to-decoy intensity ratio is 4:1.

modulation module shown in Fig. 1, we directly injected the generated states into a free-running superconducting nanowire single-photon detector and measured the probability distributions of the emitted signal and decoy states at a fixed polarization state $|H\rangle$. The measurement results are shown in Fig. 3. The temporal width of the laser is 400 ps, and the distributions of the two states almost overlap. These results are expected because the Sagnac IM is an external modulation. A similar observation was made in [45].

According to the method described in [51], we use $D_{\mu\nu} = \frac{1}{2} \text{tr} |\rho_\mu(t) - \rho_\nu(t)|$ to represent the difference between the signal and decoy states, where $\rho_\mu(t)$ and $\rho_\nu(t)$ are the quantum states in which Eve is used to distinguish the signal state and decoy state for each pulse in the time domain. Based on the probability distribution trace shown in Fig. 2, we can obtain the matrices of the signal and decoy states. The results of $\rho_\mu(t)$ and $\rho_\nu(t)$ are listed in Tab. IV. By inputting the results in Tab. IV into $D_{\mu\nu} = \frac{1}{2} \text{tr} |\rho_\mu(t) - \rho_\nu(t)|$, we obtain $D_{\mu\nu} = 1.6 \times 10^{-3}$.

3. Trojan Horse

To obtain the required parameters for characterizing the risk of Trojan-horse attacks in our system, we use a homemade single-photon optical time-domain reflectometry to measure the reflectivity of the transmitter. The measurement setup is illustrated in Fig. 4, and the resulting traces are shown in Fig. 5.

The schematic shown in Fig. 4 is as follows. A 1 MHz pulsed laser (LD₁) with a center wavelength of 1550 nm

is connected to Alice through a circulator (C). Using a digital delay generator (DG645) to uniformly change the delay of a gated single-photon detector (SPD), we can obtain the resulting traces of reflected light. The measurement results are shown in Fig. 5. Moreover, the time of the accumulated data for each step was 1 s.

The incident light intensity of the laser was -50.251 dBm, with a corresponding number of single photons of $\mu_{Eve} = 7.360 \times 10^{10}/s$. According to Fig. 5, the number of leaked $n_{leak} = 9.725 \times 10^5/s$. Here, we include all reflection peaks that cause information leakage, that is, CPM_t, J₆, BS₁, LD₂. Subsequently, we calculate the total reflectivity R_a of Alice as follows:

$$R_a = \frac{n_{leak}}{\eta_{Eve} \times \mu_{Eve}} = 1.8 \times 10^{-4}, \quad (\text{A6})$$

where $\eta_{Eve} = 7.34\%$ denotes the SPD detection efficiency. Moreover, we can estimate the worst case of leaked information due to the Trojan horse attack in our setup. Suppose that Eve could attack with a number of photons up to $\mu_{Eve}^{max} = 10^{20}/s$ [61], which is the maximum light intensity an optical device can withstand. Considering an optical isolator with an isolation value of 180.3dB in the transmitter, the Trojan-horse parameter μ_{out} is as follows:

$$\mu_{out} = \frac{R_a \times \mu_{Eve}^{max} \times 10^{-18.03}}{f_r} = 3.6 \times 10^{-10}, \quad (\text{A7})$$

$f_r = 50$ MHz is the clock frequency rate of the setup, as shown in Fig. 1.

In the experiment, we only considered the side channel leakage caused by the Trojan horse. Thus, we can express f as

$$f = \sqrt{1 - \frac{(1 - f_{th})}{\eta}} \quad (\text{A8})$$

where $\eta = \eta_c \times \eta_{Bob} \times \eta_d$, and f_{th} is the Trojan horse fidelity matrix, which can be expressed as

$$f_{th} = \begin{bmatrix} 1 & e^{-4\mu_{out}} & e^{-2\mu_{out}} & e^{-2\mu_{out}} \\ e^{-4\mu_{out}} & 1 & e^{-2\mu_{out}} & e^{-2\mu_{out}} \\ e^{-2\mu_{out}} & e^{-2\mu_{out}} & 1 & e^{-4\mu_{out}} \\ e^{-2\mu_{out}} & e^{-2\mu_{out}} & e^{-4\mu_{out}} & 1 \end{bmatrix}, \quad (\text{A9})$$

Here, we consider the upper bound of μ_{out} , and thus, we have

$$f_{th} = \begin{bmatrix} 1 & e^{-1.4 \times 10^{-9}} & e^{-7.2 \times 10^{-10}} & e^{-7.2 \times 10^{-10}} \\ e^{-1.4 \times 10^{-9}} & 1 & e^{-7.2 \times 10^{-10}} & e^{-7.2 \times 10^{-10}} \\ e^{-7.2 \times 10^{-10}} & e^{-7.2 \times 10^{-10}} & 1 & e^{-1.4 \times 10^{-9}} \\ e^{-7.2 \times 10^{-10}} & e^{-7.2 \times 10^{-10}} & e^{-1.4 \times 10^{-9}} & 1 \end{bmatrix}. \quad (\text{A10})$$

Then, we can give the side channel matrix f_{β_i} used in

TABLE IV. Probability distribution ρ_μ and ρ_ν in the time domain. We provide the normalized density matrix of the probability distribution of the pulses according to a width of 40 ps.

t (ps)	5800	5840	5880	5920	5960	6000	6040	6080	6120	6160	6200
$\rho_\mu(t)$ (10^{-4})	7.732	8.571	22.71	72.28	210.7	489.8	855.3	1165	1322	1348	1283
$\rho_\nu(t)$ (10^{-4})	7.565	8.406	22.43	71.05	211.1	486.8	851.4	1166	1322	1343	1286

t (ps)	6240	6280	6320	6360	6400	6440	6480	6520	6560	6600	6640
$\rho_\mu(t)$ (10^{-4})	1108	834.4	553.4	332.0	184.2	95.70	49.88	25.58	14.31	9.101	7.466
$\rho_\nu(t)$ (10^{-4})	1112	833.4	558.2	334.7	185.1	95.43	50.04	24.64	13.85	9.810	7.432

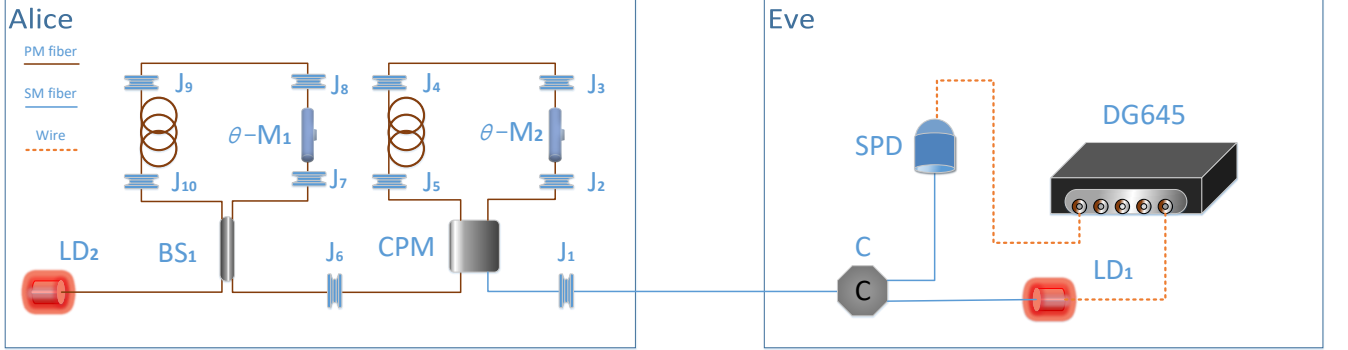


FIG. 4. Setup of Eve's Trojan-house attack. J_i : fiber flange; LD_1 : Eve's laser; LD_2 : Alice's laser; θ - M_i : phase modulator; BS_1 : beam splitter of 75:25; CPM : customized polarization module; SPD : single-photon avalanche detector; C : circulator; $DG645$: digital delay generator.

Eq. (3) as follows:

$$\begin{aligned}
 f_{z_0} &= \text{diag} [f_{(1,1)} & f_{(1,2)} & f_{(1,3)} & f_{(1,4)}] \\
 f_{z_1} &= \text{diag} [f_{(2,1)} & f_{(2,2)} & f_{(2,3)} & f_{(2,4)}] \\
 f_{x_0} &= \text{diag} [f_{(3,1)} & f_{(3,2)} & f_{(3,3)} & f_{(3,4)}] \\
 f_{x_1} &= \text{diag} [f_{(4,1)} & f_{(4,2)} & f_{(4,3)} & f_{(4,4)}],
 \end{aligned} \tag{A11}$$

where $f_{(i,j)}$ is the element in the i -th row and j -th column of the matrix f .

According to f , f_{β_i} , and Z_{ij} , we can obtain the equation for Z_{ij}^p as follows:

$$\begin{aligned}
 Z_{ij}^p &= (V_{ij}^0)^+ \cdot f \cdot V_{ij}^0 + (V_{ij}^1)^+ \cdot f \cdot V_{ij}^1 \\
 &\quad + (V_{ij}^0)^+ \cdot f \cdot V_{ij}^1 + (V_{ij}^1)^+ \cdot f \cdot V_{ij}^0,
 \end{aligned} \tag{A12}$$

where $i, j = 0, 1$, $V_{ij}^0 = \Omega_{ij}^0 \otimes f_{z_0}$, and $V_{ij}^1 = \Omega_{ij}^1 \otimes f_{z_1}$. Ω_{ij} can be expressed as follows:

$$\begin{aligned}
 \Omega_{00}^0 &= Z_{00} + Z_{01}, & \Omega_{00}^1 &= Z_{10} + Z_{11} \\
 \Omega_{01}^0 &= Z_{00} - Z_{01}, & \Omega_{01}^1 &= Z_{10} - Z_{11} \\
 \Omega_{10}^0 &= Z_{00} + Z_{01}, & \Omega_{10}^1 &= -Z_{10} - Z_{11} \\
 \Omega_{11}^0 &= Z_{00} - Z_{01}, & \Omega_{11}^1 &= -Z_{10} + Z_{11}.
 \end{aligned} \tag{A13}$$

4. Detection mismatch

Here, we consider Eve's time-shift attack [62] on Bob's detectors, which implies that Eve can randomly shift the arrival time of each signal to either t_1 or t_2 . Thus, Bob's measurement result is biased toward 0 or 1 depending on the arrival time t_1 or t_2 .

To obtain the flaw parameters $F_j^+ F_j$ and C of our system under a time-shift attack, we measured the detection efficiency of the four detectors under the same light pulse. This approach ensured the consistency of the pulse arrival time. The light intensity used in the experiment was -104.176dBm, and the gating of SPD was 1ns. By using DG645 to change the delay of SPD at 5 ps steps uniformly, we can obtain the detection efficiency curve of the four detectors. The results are shown in Fig. 6.

The measurements of the proposed system are performed using four detectors, limiting Eve's time-shift attack to some extent. In this case, Eve cannot determine Bob's basis of measurement; therefore, Eve cannot simultaneously select the optimal attack for each basis simultaneously. Eve could select large shifts in Z -basis and X -basis by a simple consideration, which would provide substantial intrinsic detection efficiency mismatches. Note that the operation of Bob to select the measurement basis is independent of Eve's time-shift attack; therefore, Eve should have the same arrival time for different bases in Fig. 6. In this case, we provide the optimal pulse ar-

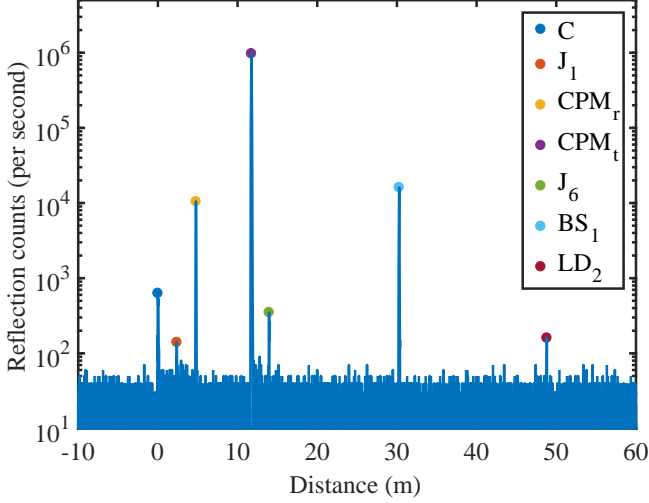


FIG. 5. Leakage peaks of the transmitter unit. The distance was measured from the reflection peak of circulator C. Note that the peaks of C, J_1 , CPM_r , J_6 , and LD_2 are reflections from the end face of the device. However, the peaks of CPM_t and BS_1 are the transmitted light due to the Trojan light entering the CPM or BS_1 after being transmitted in the Sagnac loop.

rival time of Eve by considering the detection mismatch between the Z -basis and the X -basis. The detection efficiencies of the four detectors at $t_1 = -300$ and $t_2 = 375$ are listed in Tab. VI.

We define H and P polarization states as bit “0” and V and M polarization states as bit “1”. Moreover, the probability of choosing the Z -basis is 90%. Based on the values listed in Tab. VI, we can obtain the detection efficiency matrix F_j used in Eq. (3),

$$F_j = 0.9 \times F_{z_j} + 0.1 \times F_{x_j}, \quad (\text{A14})$$

here F_{z_j} and F_{x_j} are the normalized matrices of detection efficiency of bit “ j ” in the Z -basis and X -basis respectively, which can be expressed as follows:

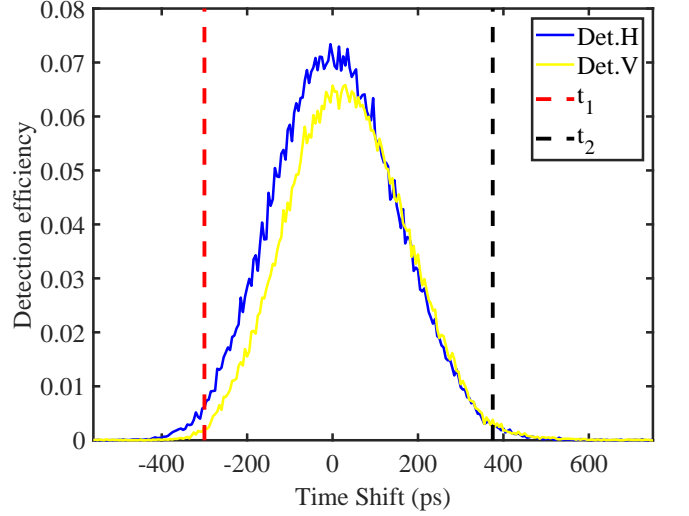
$$\begin{aligned} F_{z_0} &= \begin{bmatrix} 1 & 0 \\ 0 & \frac{\eta_H(t_2)}{\eta_V(t_2)} \end{bmatrix} & F_{z_1} &= \begin{bmatrix} \frac{\eta_V(t_1)}{\eta_H(t_1)} & 0 \\ 0 & 1 \end{bmatrix} \\ F_{x_0} &= \begin{bmatrix} 1 & 0 \\ 0 & \frac{\eta_P(t_2)}{\eta_M(t_2)} \end{bmatrix} & F_{x_1} &= \begin{bmatrix} \frac{\eta_M(t_1)}{\eta_P(t_1)} & 0 \\ 0 & 1 \end{bmatrix}. \end{aligned} \quad (\text{A15})$$

By substituting the detection efficiencies listed in Tab. VI into Eq. (A14) and Eq. (A15), we can obtain F_0 and F_1 such that

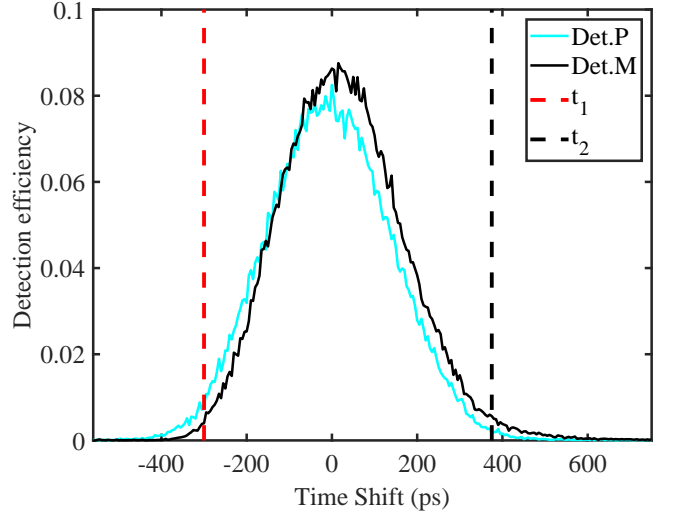
$$F_0 = \begin{bmatrix} 1 & 0 \\ 0 & 0.8137 \end{bmatrix} \quad F_1 = \begin{bmatrix} 0.5791 & 0 \\ 0 & 1 \end{bmatrix}. \quad (\text{A16})$$

Subsequently, we can use F_0 and F_1 to construct C in Eq. (3). First, we build an auxiliary matrix CF as follows:

$$CF = F_0 (F_1 + F_0)^{-1} F_0. \quad (\text{A17})$$



(a)



(b)

FIG. 6. Efficiencies of four detectors versus time shifts. (a) Detection efficiency of the Z -basis, blue and yellow lines represent the detector H and detector V. (b) Detection efficiency on the X -basis, cyan and black lines represent the detector P and detector M. t_1 (dashed red line) = -300 ps and t_2 (dashed black line) = 375 ps are the optimal shift times for the attack.

All eigenvectors and eigenvalues of CF are composed of V and D ,

$$\begin{aligned} D &= \text{diag} [\lambda_1 \ \lambda_2 \ \cdots \ \lambda_n] \\ V &= [\varphi_1 \ \varphi_2 \ \cdots \ \varphi_n], \end{aligned} \quad (\text{A18})$$

where λ_n is the n -th eigenvalue of matrix CF , and φ_n is the n -th eigenvector. Then, C can be expressed as follows:

$$C = V^+ F_0 \sqrt{\min \left[\frac{1}{D}, \text{diag}(n) \right]}, \quad (\text{A19})$$

TABLE V. Experimental raw counts. $n_{\beta,k}$ and $m_{\beta,k}$ are the detection and error detection events on the β -basis with a specific intensity $k \in \{\mu, \nu\}$. $n_{\beta_i,k}$ and $m_{\beta_i,k}$ are the parts of $n_{\beta,k}$ and $m_{\beta,k}$ that Alice sends encoded as a bit “ i ” pulse, $i \in 0, 1$. $N_{\beta,\beta'}$ is the total number of pulses that Alice sends the quantum state in β -basis and Bob successfully detects in the β' -basis. $N_{\beta_i,\beta'}$ represents the counts when the total number of pulses that Alice sends the quantum state in the β -basis with bit “ i ” and Bob detects in the β' -basis, $\beta, \beta' \in \{z, x\}$.

$L(km)$	$n_{z0,\mu}$	$m_{z0,\mu}$	$n_{z1,\mu}$	$m_{z1,\mu}$	$n_{x0,\mu}$	$m_{x0,\mu}$	$n_{x1,\mu}$	$m_{x1,\mu}$	$n_{z,\mu}$	$m_{z,\mu}$	$N_{zz}(10^9)$	$N_{z0z}(10^9)$	$N_{z1z}(10^9)$
25	55776166	549127	59132433	670342	635779	7764	641408	5836	114908599	1219469	8.1529	4.0764	4.0764
50	13572261	147390	15000021	133335	137787	1708	169011	2109	28572282	280725	8.1296	4.0648	4.0648
75	4576860	54744	3828257	50017	72260	1310	76612	1600	8405117	104761	8.1390	4.0695	4.0695

$L(km)$	$n_{z0,\nu}$	$m_{z0,\nu}$	$n_{z1,\nu}$	$m_{z1,\nu}$	$n_{x0,\nu}$	$m_{x0,\nu}$	$n_{x1,\nu}$	$m_{x1,\nu}$	$n_{z,\nu}$	$m_{z,\nu}$	$N_{xx}(10^7)$	$N_{x0x}(10^7)$	$N_{x1x}(10^7)$
25	3192913	84869	2166169	29448	33203	825	34917	514	5359082	114317	10.065	5.0326	5.0226
50	1185426	27400	961101	9283	18647	549	11265	177	2146527	36683	10.036	5.0182	5.0182
75	1078178	17235	965843	17583	13072	458	12381	387	2044021	34818	10.048	5.0240	5.0240

TABLE VI. Detection efficiency in t_1 and t_2 . η_H, η_V, η_P , and η_M are the detection efficiencies of detectors H, V, P, and M, respectively. Moreover, t_1 and t_2 are the pulse arrival times.

	t_1	t_2		t_1	t_2
$\eta_H(t)$	0.55%	0.33%	$\eta_P(t)$	0.71%	0.18%
$\eta_V(t)$	0.31%	0.38%	$\eta_M(t)$	0.51%	0.56%

where $diag(n)$ is a unitary diagonal matrix equal to dimension D .

Appendix B: Experimental data

Detailed experimental data are listed in Tab. V.

- [1] H.-K. Lo and H. F. Chau, *Science* **283**, 2050 (1999).
- [2] P. W. Shor and J. Preskill, *Phys. Rev. Lett.* **85**, 441 (2000).
- [3] D. Gottesman, H.-K. Lo, N. Lütkenhaus, and J. Preskill, *Quant. Inf. Comput.* **4**, 325 (2004).
- [4] Y. Liu, T.-Y. Chen, J. Wang, W.-Q. Cai, X. Wan, L.-K. Chen, J.-H. Wang, S.-B. Liu, H. Liang, L. Yang, C.-Z. Peng, K. Chen, Z.-B. Chen, and J.-W. Pan, *Opt. Express* **18**, 8587 (2010).
- [5] S. Wang, W. Chen, J.-F. Guo, Z.-Q. Yin, H.-W. Li, Z. Zhou, G.-C. Guo, and Z.-F. Han, *Opt. Lett.* **37**, 1008 (2012).
- [6] Z. Yuan, A. Plews, R. Takahashi, K. Doi, W. Tam, A. W. Sharpe, A. R. Dixon, E. Lavelle, J. F. Dynes, A. Murakami, M. Kujiraoka, M. Lucamarini, Y. Tanizawa, H. Sato, and A. J. Shields, *J. Lightwave Technol.* **36**, 3427 (2018).
- [7] A. Boaron, G. Boso, D. Rusca, C. Vulliez, C. Autebert, M. Caloz, M. Perrenoud, G. Gras, F. Bussi eres, M.-J. Li, D. Nolan, A. Martin, and H. Zbinden, *Phys. Rev. Lett.* **121**, 190502 (2018).
- [8] C. Agnesi, M. Avesani, L. Calderaro, A. Stanco, G. Folletto, M. Zahidy, A. Scriminich, F. Vedovato, G. Vallone, and P. Villoresi, *Optica* **7**, 284 (2020).
- [9] X.-Y. Zhou, H.-J. Ding, M.-S. Sun, S.-H. Zhang, J.-Y. Liu, C.-H. Zhang, J. Li, and Q. Wang, *Phys. Rev. Appl.* **15**, 064016 (2021).
- [10] H. Takenaka, A. Carrasco-Casado, M. Fujiwara, M. Kitamura, M. Sasaki, and M. Toyoshima, *Nature Photon.* **11**, 502 (2017).
- [11] S.-K. Liao, W.-Q. Cai, L. Zhang, Y. Li, J. Wang, J. Yin, Q. Shen, Y. Cao, Z.-P. Li, F.-Z. Li, X.-W. Chen, L.-H. Sun, J.-J. Jia, J.-C. Wu, X.-J. Jiang, F.-J. Wang, Y.-M. Huang, Q. Wang, and J.-W. Pan, *Nature*, 43 (2017).
- [12] H. Chen, J. Wang, B. Tang, Z. Li, B. Liu, and S. Sun, *Opt. Lett.* **45**, 3022 (2020).
- [13] M. Peev, C. Pacher, R. All eume, C. Barreiro, J. Bouda, W. Boxleitner, T. Debuisschert, E. Diamanti, M. Dianati, J. F. Dynes, S. Fasel, S. Fossier, M. F urst, J. D. Gautier, O. Gay, N. Gisin, P. Grangier, A. Happe, Y. Hasani, M. Hentschel, H. H ubel, G. Humer, T. L anger, M. Legr e, R. Lieger, J. Lodewyck, T. Lor unser, N. L utkenhaus, A. Marhold, T. Matyus, O. Maurhart, L. Monat, S. Nauerth, J. B. Page, A. Poppe, E. Querasser, G. Ribordy, S. Robyr, L. Salvail, A. W. Sharpe, A. J. Shields, D. Stucki, M. Suda, C. Tamas, T. Themel, R. T. Thew, Y. Thoma, A. Treiber, P. Trinkler, R. Tualle-Brouiri, F. Vannel, N. Walenta, H. Weier, H. Weinfurter, I. Wimberger, Z. L. Yuan, H. Zbinden, and A. Zeilinger, *New J. Phys.* **11**, 075001 (2009).
- [14] T.-Y. Chen, J. Wang, H. Liang, W.-Y. Liu, Y. Liu, X. Jiang, Y. Wang, X. Wan, W.-Q. Cai, L. Ju, L.-K. Chen, L.-J. Wang, Y. Gao, K. Chen, C.-Z. Peng, Z.-B. Chen, and J.-W. Pan, *Opt. Express* **18**, 27217 (2010).
- [15] M. Sasaki, M. Fujiwara, H. Ishizuka, W. Klaus, K. Wakui, M. Takeoka, S. Miki, T. Yamashita, Z. Wang, and A. Tanaka, *Opt. Express* **19**, 10387 (2011).
- [16] S. Wang, W. Chen, Z.-Q. Yin, H.-W. Li, D.-Y. He, Y.-H. Li, Z. Zhou, X.-T. Song, F.-Y. Li, D. Wang, H. Chen, Y.-G. Han, J.-Z. Huang, J.-F. Guo, P.-L. Hao, M. Li, C.-M. Zhang, D. Liu, W.-Y. Liang, C.-H. Miao, P. Wu, G.-C. Guo, and Z.-F. Han, *Opt. Express* **22**, 21739 (2014).
- [17] J. F. Dynes, A. Wonfor, W. W. S. Tam, A. W. Sharpe, R. Takahashi, M. Lucamarini, A. Plews, Z. L. Yuan, A. R. Dixon, J. Cho, Y. Tanizawa, J. P. Elbers, H. Grei er, I. H. White, R. V. Penty, and A. J. Shields, *Npj Quantum Inf.* **5**, 101 (2019).

- [18] Y.-A. Chen, Q. Zhang, T.-Y. Chen, W.-Q. Cai, S.-K. Liao, J. Zhang, K. Chen, J. Yin, J.-G. Ren, Z. Chen, S.-L. Han, Q. Yu, K. Liang, F. Zhou, X. Yuan, M.-S. Zhao, T.-Y. Wang, X. Jiang, L. Zhang, W.-Y. Liu, Y. Li, Q. Shen, Y. Cao, C.-Y. Lu, R. Shu, J.-Y. Wang, L. Li, N.-L. Liu, F. Xu, X.-B. Wang, C.-Z. Peng, and J.-W. Pan, *Nature* **589**, 214 (2021).
- [19] S. Wang, Z.-Q. Yin, D.-Y. He, W. Chen, R.-Q. Wang, P. Ye, Y. Zhou, G.-J. Fan-Yuan, F.-X. Wang, W. Chen, Y.-G. Zhu, P. V. Morozov, A. V. Divochiy, Z. Zhou, G.-C. Guo, and Z.-F. Han, *Nature Photon.* (2022), [10.1038/s41566-021-00928-2](https://doi.org/10.1038/s41566-021-00928-2).
- [20] M. Lucamarini, Z. L. Yuan, J. F. Dynes, and A. J. Shields, *Nature* **557**, 400 (2018).
- [21] D. Gottesman, H.-K. Lo, N. Lütkenhaus, and J. Preskill, *Quantum Inf. Comput.* **4**, 325 (2004).
- [22] L. Lydersen, C. Wiechers, C. Wittmann, D. Elser, J. Skaar, and V. Makarov, *Nature Photon.* **4**, 801 (2010).
- [23] Y.-J. Qian, D.-Y. He, S. Wang, W. Chen, Z.-Q. Yin, G.-C. Guo, and Z.-F. Han, *Phys. Rev. Appl.* **10**, 064062 (2018).
- [24] K.-i. Yoshino, M. Fujiwara, K. Nakata, T. Sumiya, T. Sasaki, M. Takeoka, M. Sasaki, A. Tajima, M. Koashi, and A. Tomita, *Npj Quantum Inf.* **4**, 8 (2018).
- [25] K. Wei, W. Zhang, Y.-L. Tang, L. You, and F. Xu, *Phys. Rev. A* **100**, 022325 (2019).
- [26] A. Huang, R. Li, V. Egorov, S. Tchouragoulov, K. Kumar, and V. Makarov, *Phys. Rev. Appl.* **13**, 034017 (2020).
- [27] X.-L. Pang, A.-L. Yang, C.-N. Zhang, J.-P. Dou, H. Li, J. Gao, and X.-M. Jin, *Phys. Rev. Appl.* **13**, 034008 (2020).
- [28] H.-K. Lo, M. Curty, and K. Tamaki, *Nature Photon.* **8**, 595 (2014).
- [29] F. Xu, X. Ma, Q. Zhang, H.-K. Lo, and J.-W. Pan, *Rev. Mod. Phys.* **92**, 025002 (2020).
- [30] S. Pirandola, U. L. Andersen, L. Banchi, M. Berta, D. Bunandar, R. Colbeck, D. Englund, T. Gehring, C. Lupo, C. Ottaviani, J. L. Pereira, M. Razavi, J. Shamsul Shaari, M. Tomamichel, V. C. Usenko, G. Vallone, P. Villaresi, and P. Wallden, *Adv. Opt. Photonics* **12**, 1012 (2020).
- [31] S. Sun and A. Huang, *Entropy* **24**, 260 (2022).
- [32] A. Acín, N. Brunner, N. Gisin, S. Massar, S. Pironio, and V. Scarani, *Phys. Rev. Lett.* **98**, 230501 (2007).
- [33] R. Schwonnek, K. T. Goh, I. W. Primaatmaja, E. Y. Z. Tan, R. Wolf, V. Scarani, and C. C. W. Lim, *Nat. Commun.* **12**, 2880 (2021).
- [34] F. Xu, Y.-Z. Zhang, Q. Zhang, and J.-W. Pan, *Phys. Rev. Lett.* **128**, 110506 (2022).
- [35] H.-K. Lo, M. Curty, and B. Qi, *Phys. Rev. Lett.* **108**, 130503 (2012).
- [36] S. L. Braunstein and S. Pirandola, *Phys. Rev. Lett.* **108**, 130502 (2012).
- [37] C.-h. F. Fung, K. Tamaki, B. Qi, H.-K. Lo, and X. Ma, *Quantum Info. Comput.* **9**, 131 (2009).
- [38] Y. Zhang, P. J. Coles, A. Winick, J. Lin, and N. Lütkenhaus, *Phys. Rev. Research* **3**, 013076 (2021).
- [39] Z.-Q. Yin, C.-H. F. Fung, X. Ma, C.-M. Zhang, H.-W. Li, W. Chen, S. Wang, G.-C. Guo, and Z.-F. Han, *Phys. Rev. A* **88**, 062322 (2013).
- [40] K. Tamaki, M. Curty, G. Kato, H.-K. Lo, and K. Azuma, *Phys. Rev. A* **90**, 052314 (2014).
- [41] M. Pereira, M. Curty, and K. Tamaki, *Npj Quantum Inf.* **5**, 62 (2019).
- [42] M. Pereira, G. Kato, A. Mizutani, M. Curty, and K. Tamaki, *Sci. Adv.* **6**, eaaz4487 (2020).
- [43] M. Lucamarini, I. Choi, M. B. Ward, J. F. Dynes, Z. L. Yuan, and A. J. Shields, *Phys. Rev. X* **5**, 031030 (2015).
- [44] C. Li, M. Curty, F. Xu, O. Bedrova, and H.-K. Lo, *Phys. Rev. A* **98**, 042324 (2018).
- [45] A. Huang, S.-H. Sun, Z. Liu, and V. Makarov, *Phys. Rev. A* **98**, 012330 (2018).
- [46] F. Xu, K. Wei, S. Sajeed, S. Kaiser, S. Sun, Z. Tang, L. Qian, V. Makarov, and H.-K. Lo, *Phys. Rev. A* **92**, 032305 (2015).
- [47] Z. Tang, K. Wei, O. Bedrova, L. Qian, and H.-K. Lo, *Phys. Rev. A* **93**, 042308 (2016).
- [48] C. Wang, S. Wang, Z.-Q. Yin, W. Chen, H.-W. Li, C.-M. Zhang, Y.-Y. Ding, G.-C. Guo, and Z.-F. Han, *Opt. Lett.* **41**, 5596 (2016).
- [49] X.-Y. Zhou, H.-J. Ding, C.-H. Zhang, J. Li, C.-M. Zhang, and Q. Wang, *Opt. Lett.* **45**, 4176 (2020).
- [50] C. Huang, Y. Chen, L. Jin, M. Geng, J. Wang, Z. Zhang, and K. Wei, *Phys. Rev. A* **105**, 012421 (2022).
- [51] S. Sun and F. Xu, *New J. Phys.* **23**, 023011 (2021).
- [52] D. Rusca, A. Boaron, F. Grünenfelder, A. Martin, and H. Zbinden, *Appl. Phys. Lett.* **112**, 171104 (2018).
- [53] H.-K. Lo, X. Ma, and K. Chen, *Phys. Rev. Lett.* **94** (2005), [10.1103/PhysRevLett.94.230504](https://doi.org/10.1103/PhysRevLett.94.230504).
- [54] X.-B. Wang, *Phys. Rev. Lett.* **94**, 230503 (2005).
- [55] P. J. Coles, E. M. Metodiev, and N. Lütkenhaus, *Nat. Commun.* **7**, 11712 (2016).
- [56] A. Winick, N. Lütkenhaus, and P. J. Coles, *Quantum* **2**, 77 (2018).
- [57] D. Ma, X. Liu, C. Huang, H. Chen, H. Lin, and K. Wei, *Opt. Lett.* **46**, 2152 (2021).
- [58] K. Tamaki, M. Curty, G. Kato, H.-K. Lo, and K. Azuma, *Phys. Rev. A* **90**, 052314 (2014).
- [59] P. Sibson, C. Erven, M. Godfrey, S. Miki, T. Yamashita, M. Fujiwara, M. Sasaki, H. Terai, M. G. Tanner, C. M. Natarajan, R. H. Hadfield, J. L. O'Brien, and M. G. Thompson, *Nat. Commun.* **8**, 13984 (2017).
- [60] C. Ma, W. D. Sacher, Z. Tang, J. C. Mikkelsen, Y. Yang, F. Xu, T. Thiessen, H.-K. Lo, and J. K. S. Poon, *Optica* **3**, 1274 (2016).
- [61] H. Tan, W. Li, L. Zhang, K. Wei, and F. Xu, *Phys. Rev. Appl.* **15**, 064038 (2021).
- [62] Y. Zhao, C.-H. F. Fung, B. Qi, C. Chen, and H.-K. Lo, *Phys. Rev. A* **78**, 042333 (2008).
- [63] Á. Navarrete and M. Curty, *Quantum Sci. Technol.* **7**, 035021 (2022).